Hierarchical Predictive Control of Microgrids in Islanded Operation

Alessio La Bella, Stefano Raimondi Cominesi, Carlo Sandroni, and Riccardo Scattolini

***Abstract*— This paper presents a hierarchical control architecture for the regulation of frequency and nodal voltages of a microgrid in islanded operation. Considering systems with both dispatchable and nondispatchable generation, as well as noncontrollable loads, the suggested approach allows to coordinate the MG devices in order to maintain the network variables inside the desired operational ranges. Moreover, the proposed algorithm, based on model predictive control, introduces the possibility to define different resource management strategies while taking into account the constraints of the available devices. Simulation examples are reported and described in the final part of this paper.**

***Note to Practitioners*—This paper proposes a method to control the nodal voltages and the frequency of a microgrid (MG) in islanded operation. The implementation of this control scheme requires defining a control logic for the inverters connecting the distributed generation units to the MG. A centralized supervising system has also to be deployed for the coordination of their actions. This paper shows how the flexibility of this structure allows for the implementation of different resource management strategies.**

***Index Terms*— Frequency control, power generation control, predictive control, voltage control.**

I. Introduction

THE NEED of reducing CO_2 emissions due to energy generation, as well as the need of more efficient and reliable electrical systems, has led to an increasing diffusion of *distributed energy resources* (DER) and, with that, to a growing research interest on the topic. The actual electric infrastructure is expected to evolve to a more flexible and distributed electrical framework of low-voltage small-scale grids, called *microgrids* (MG), all interconnected to a large-scale electric power backbone. An MG can be identified as a self-contained cluster of dispatchable microgenerators, renewable sources, loads, and storage units. Being a site of both energy production and consumption, an MG may also operate in islanded mode, where it is no longer supported by the main grid, but it relies only on its generation sources. The islanded operation could be planned for economical reasons, or it could occur spontaneously if a fault triggers the disconnection of the MG. This condition requires an efficient and proper coordination of the system, since peaks of power demand do not necessarily coincide with generation peaks given the nondeterministic and intermittent production of some sources. Network frequency and line-to-line voltages must be also taken into account as they are extremely sensitive to the uncertain power variations and could diverge under unbalanced power conditions. It should be noted that, unlike today power systems where the high number of synchronous generators ensures a large system inertia, MGs are likely to be characterized by low inertia as most distributed generation sources are connected to the MG network through electronically controlled inverters. This interface is necessary, since some microgeneration units directly produce dc power, such as photovoltaics and batteries, while others generate asynchronous ac power, like wind turbines. Although the inverter interconnection enhances the dynamic performance, the lack of directly connected high-inertia rotating generators makes the system more critical as fast voltage or frequency deviations may occur, especially if the MG is not supported by a synchronous host grid.

The mentioned issues may be overcame through the introduction of a supervising control system regulating the output powers of the generation units. Given the electrical complexity and extension of an MG, as well as the need of a high-level coordination of the units, the hierarchical control structure is the best framework for the MG control scheme [1]. This structure usually consists in three layers: the *primary*, the *secondary*, and the *tertiary* controller. The primary level generally corresponds to a proportional decentralized controller performing a fast control action, so that the voltages and frequency deviations are quickly reduced. Although this layer manages to avoid the instability of the system, a sole proportional action can neither restore the network variables to their nominal values nor perform a high-level coordination among the generators. This motivates the introduction of additional levels to the hierarchical control structure, i.e., the *secondary* and *tertiary layers*. The former is usually designed to restore the network variables to their nominal values acting on the primary controllers' references, while the latter, operating in the order of several minutes or hours, is typically designed to optimize the power flows between the MG and the main grid. It is worth noticing that the third control layer may be

Manuscript received July 8, 2016; revised November 7, 2016; accepted November 8, 2016. Date of publication December 28, 2016; date of current version April 5, 2017. This paper was recommended for publication by Associate Editor S. Grammatico and Editor N. Ciulli upon evaluation of the reviewers' comments.

A. La Bella, S. Raimondi Cominesi, and R. Scattolini are with the Dipartimento di Elettronica, Informazione e Bioingegneria, Politecnico di Milano, 20133 Milan, Italy (e-mail: alessio.labella@polimi.it; stefano.raimondi@polimi.it; riccardo.scattolini@polimi.it).

C. Sandroni is with RSE S.p.A., 20134 Milan, Italy (e-mail: carlo.sandroni@rse-web.it).

Color versions of one or more of the figures in this paper are available online at http://ieeexplore.ieee.org.

Digital Object Identifier 10.1109/TASE.2016.2633397

needed only in grid-connected mode, while during the islanded operation, the highest coordination can be usually performed by the secondary controller.

The recent interest in islanded MGs' management has motivated many research activities concerning the definition and analysis of their control system. With regard to the primary control, the so-called *droop control* [2] has attracted the most attention. Although its stability properties rarely have been rigorously analyzed given the complexity of an inverter-based MG ([3], [4] whose considerations hold true under certain assumptions), several studies have been carried out [5]–[8], proving the effectiveness of this control strategy in stabilizing the MG network variables. As above-mentioned, though, droop control leads to steady-state deviations, since it only relies on a proportional control action. Because of this, in [9], a distributed secondary scheme, called distributed averaging proportional integral controller, was devised to include integral action so as to eliminate steady-state frequency and voltage offsets, while preserving the power sharing performed by the primary control. Other interesting examples of distributed secondary control layers, implemented using multiagent or consensus techniques, may also be found in [10]–[12]. Despite representing a more flexible and simpler structure, however, a distributed control architecture cannot provide the high level of coordination typical of centralized approaches.

Centralized secondary control methods have also been discussed in the literature, such as in [13] and [14], but it is rarely the case that an efficient control scheme accounting for both network variables regulation and optimal power management has been developed for the islanded condition. Moreover, the increasing diffusion of electric energy storages, rarely discussed, further supports the necessity of an efficient coordination among the devices and introduces the need to account for their states of charge (SOCs). For all these reasons, this paper proposes a novel control structure for islanded MG operation, devised to maintain the network variables inside the desired operational ranges while, at the same time, providing the flexibility and coordination necessary to implement different resource management strategies and account for the energy storages' reserves.

Specifically, similar to the regulating structure adopted for the main distribution networks, we propose a hierarchical control architecture: a *primary control* layer is entitled to modulate the DER units power production in order to limit any deviation of frequency and voltages from their nominal values. A *secondary control* is consequently introduced with the aim to return the network to its nominal conditions. The primary layer consists in a decentralized droop control scheme, running at a faster time scale with respect to the secondary centralized control system, based on a model predictive control (MPC) algorithm. The choice of this scheme also allows to optimally distribute the power production of the controllable units taking into account some predictions, if available, of the nondispatchable power profiles (renewable sources, loads, and so on) as well as to implement different resource management strategies by properly tuning the MPC cost function. This paper is structured as follows. In Section II, the hierarchical control structure is presented. Section III shows the performance of the control strategy here presented in different case-scenario simulations. Finally, some conclusions are drawn in Section IV.

II. Hierarchical Control Strategy

This Section is devoted to the description of the main components of the proposed control scheme. The primary control layer, presented in Section II-A, consists in a distributed control system, based on a droop technique, locally implemented on the inverters acting as interface between the generation units and the MG with a control loop of few milliseconds. The secondary layer, designated to restore the network frequency to the desired value, and to maintain the voltages in the acceptable range, is instead described in Section II-B, and it is characterized by a longer sampling period, τ_s. In the following, we consider $\tau_s = 1$ min.

A. Primary Control Layer

An MG in islanded operation may be represented by a connected and undirect graph $\mathcal{G} = (\mathcal{V}, \mathcal{E})$, where $\mathcal{V}$ denotes the set of buses (i.e., nodes), and $\mathcal{E} \subseteq \mathcal{V} \times \mathcal{V}$ defines the set of distribution lines (i.e., edges) connecting the buses of the network. Each of the $n = |\mathcal{V}|$ buses may be characterized by the presence of a generation unit (dispatchable or not), a load, both, or neither. We define the subsets $\mathcal{V}^{Gd}$, $\mathcal{V}^{Gn}$, and $\mathcal{V}^{L}$ composed by the nodes where, respectively, dispatchable or nondispatchable generators, or loads are connected. The subset of the nodes connected to a generic generator is also defined as $\mathcal{V}^{G} := \mathcal{V}^{Gd} \cup \mathcal{V}^{Gn}$.

From a simple balance, we define the power injected at the ith node as

$$P_i = {P_i}^G + {P_i}^L \quad Q_i = {Q_i}^G + {Q_i}^L \tag{1}$$

where P and Q denote the active and reactive power, and the superscripts G and L stand, respectively, for the contribution of generation units and loads eventually connected to the bus, therefore, $\forall i = 1, \ldots, n$, it holds

$${P_i}^G = {Q_i}^G = 0, \quad \text{if } i \notin \mathcal{V}^G$$

and

$${P_i}^L = {Q_i}^L = 0, \quad \text{if } i \notin \mathcal{V}^L.$$

The well-known bus power injection approach [15] provides another formulation for the power injection at bus i as a function of the network structure and variables. Let ω be the unique frequency of the synchronous network and identify $y_i(\omega)$ with the corresponding self-admittance of the ith bus, while $y_{ij}(\omega)$ represents the admittance of the generic edge $(i, j) \in \mathcal{E}$. The elements of the *admittance matrix* $Y(\omega)$ are then defined as

$$Y_{ij}(\omega) = \begin{cases} y_i(\omega) + \displaystyle\sum_{k=1, k\neq i}^{n} y_{ik}(\omega), & \text{if } i = j \\ -y_{ij}(\omega), & \text{otherwise.} \end{cases}$$

The power injected (negative if absorbed) at the ith node may, hence, be expressed as

$$\begin{cases} P_i(V,\theta,\omega) = V_i \sum_{j=1}^{n} V_j |Y_{ij}(\omega)| \cos\left(\theta_i - \theta_j - \angle Y_{ij}(\omega)\right) \\ Q_i(V,\theta,\omega) = V_i \sum_{j=1}^{n} V_j |Y_{ij}(\omega)| \sin\left(\theta_i - \theta_j - \angle Y_{ij}(\omega)\right) \end{cases} \tag{2}$$

where $V = [V_1, V_2, \ldots, V_n]^T$ and $\theta = [\theta_1, \theta_2, \ldots, \theta_n]^T$, respectively, represent the magnitude and the phase of the voltage measured at the buses. The system of equations in (2) represents one of the possible formulations of the power flow equations, and it shows how any change in the power injected at one of the nodes affects all the network variables.

The main purpose of the primary control layer is to rapidly counteract the effect of the fluctuations due to the presence in the grid of nonpredictable loads and nondispatchable generation. This is fundamental for MGs in islanded condition, since the inverter units, commonly used as interface between the production devices and the MG network, do not provide any inherent physical relation between frequency, voltages, and power production, as rotor inertia does for rotating generators. Since any unbalance between generated and absorbed power poses a threat for the MG, the generators' output powers should be varied according to the network variables' deviations from the nominal values. To do that, we consider to equip the inverter units connected to the generation devices with a *droop control* system. Although different droop approaches exist [16], the *inverse droop* strategy is adopted, which proved to be effective in many experimental tests carried out at the RSE research center [17]. This configuration, given the set points $\bar{P}_i{}^G$ and $\bar{Q}_i{}^G$, introduces the compensation terms, $\hat{P}_i{}^G$ and $\hat{Q}_i{}^G$, so that the generated powers are varied according to the value of the network variables at the node, thus

$$\begin{aligned} P_i{}^G(V_i,\omega_i) &= \bar{P}_i{}^G + \hat{P}_i{}^G(V_i,\omega_i) \\ Q_i{}^G(V_i,\omega_i) &= \bar{Q}_i{}^G + \hat{Q}_i{}^G(V_i,\omega_i) \end{aligned} \tag{3}$$

where V_i and ω_i represent the measured values of nodal line voltage and frequency. The droop control action is meant to counteract the effect that the power unbalances have on the network variables. Since such effect is strongly related to the characteristic of the network, different droop control laws have been devised. In particular, defining the desired nominal values of nodal voltage and frequency as $V_i{}^*$ and ω^*, we adopt the droop functions

$$\hat{P}_i{}^G = m_i{}^{P\omega}(\omega_i - \omega^*) \quad \hat{Q}_i{}^G = m_i{}^{QV}\left(V_i - V_i{}^*\right)$$

for network with mainly *inductive* characteristic. In the case of *resistive* networks, instead, the frequency dynamics is more significantly influenced by the reactive power production, and the droop control actions are defined as follows:

$$\hat{P}_i{}^G = m_i{}^{PV}\left(V_i - V_i{}^*\right) \quad \hat{Q}_i{}^G = m_i{}^{Q\omega}(\omega_i - \omega^*). \tag{4}$$

The *droop coefficients* $m_i{}^{P\omega}$ and $m_i{}^{QV}$ and $m_i{}^{PV}$ and $m_i{}^{Q\omega}$ are computed so that the power production may span over the full range of the capability curve of the device (generically defined as $[P_i{}^{\min}, P_i{}^{\max}] \times [Q_i{}^{\min}, Q_i{}^{\max}]$). Thus, for the coefficient in (4), we have

$$m_i{}^{PV} = -\frac{P_i{}^{\max} - P_i{}^{\min}}{V_i{}^{\max} - V_i{}^{\min}} \quad m_i{}^{Q\omega} = \frac{Q_i{}^{\max} - Q_i{}^{\min}}{\omega_i{}^{\max} - \omega_i{}^{\min}} \tag{5}$$

with $[V_i{}^{\min}, V_i{}^{\max}]$ and $[\omega_i{}^{\min}, \omega_i{}^{\max}]$ defining the acceptable ranges for the network variables behavior.

From now on, it will be assumed that the droop control action is properly tuned, so that the network variables controlled by the primary layer converge to steady-state values satisfying (2). This is a common hypothesis, even if often not explicitated. Few works made significant contribution on this topic [4], [18] considering, though, a different network setup compared with the one discussed here. Remarkably, however, this assumption is consistent with results, and tests put in place on the real MG available at the RSE research center [17], [19].

B. Secondary Control Layer

The secondary control layer has the purpose to return the network frequency to its nominal value ω^* while minimizing the voltages' deviations. To this goal, we designed a centralized MPC structure capable to effectively coordinate the action of the dispatchable units while allowing for an efficient energy management.

Let $x = [V^\top \ \theta^\top \ \omega]^\top$ be the vector of the network variables, with θ representing the vector of voltage phase shifts with respect to a designated bus, denoted as *slack bus* (e.g., $\theta_i = \angle V_i - \angle V_n \forall i = 1, \ldots, n-1$), and let $u = [P_1, \ldots, P_n, Q_1, \ldots, Q_n]^\top$ define the vertical concatenation of both the active and reactive powers injected at the n buses of the network. Accordingly, recalling the notation adopted in Section II-A, we introduce the terms u^G and u^L as the vectors collecting both the active and reactive powers injected at each node of the MG from generation units and loads, respectively. Analogously, we let u^{Gd}, u^{Gn} identify the contribution of dispatchable and nondispatchable generators, so that $u^G = u^{Gd} + u^{Gn}$.

Without loss of generality, we also divide u^L, in two terms according to their dependence on the network variables. Adopting a notation similar to the one in (3), and explicating the dependence from x, it is possible to write

$$u^L(x) = \bar{u}^L + \hat{u}^L(x) \tag{6}$$

where $\bar{u}^L$ represents a vector of constant-power loads, while the contribution of the loads depending on the network variables, e.g., constant impedance loads, are collected in $\hat{u}^L(x)$.

In the design of the secondary controller, it is standard to assume that the inner and fast control loop is at the steady state. Combining (1)–(3) and (6), it is therefore possible to obtain the set of $2n$ nonlinear equations expressed in $2n$ unknowns that define the relationship between the variables of an islanded MG, subject to the control law in (3)

$$\bar{u} = u(x) - (\hat{u}^G(x) + \hat{u}^L(x)) \tag{7}$$

where the newly defined term $\bar{u}$ collects both the set point for the droop-controlled systems $\bar{u}^G$ and the constant-power

loads $\bar{u}^L$, that is

$$\bar{u} = \bar{u}^G + \bar{u}^L$$

and $\hat{u}^G(x) = [\hat{P}_i^G(x)^\top \ \hat{Q}_i^G(x)^\top]^\top$ is the vector collecting all the droop compensation terms.

Let $\mathcal{J}(x)$ be the jacobian of $\bar{u}(x)$, and $\mathcal{S}$ the corresponding sensitivity matrix, computed, according to a common approach [20]–[22] as $\mathcal{S} = \mathcal{J}^{-1}$, recalling (7), one has

$$\mathcal{J}(x) = \frac{d\bar{u}}{dx} = \tilde{\mathcal{J}}(x) - \mathcal{J}^G(x) - \mathcal{J}^L(x) \tag{8}$$

where $\tilde{\mathcal{J}}(x)$ depends only on the network structure and parameters through (2), and $\mathcal{J}^G(x)$, $\mathcal{J}^L(x)$ are defined as follows:

$$\mathcal{J}^G(x_0) = \begin{bmatrix} \left.\frac{\partial \hat{P}^G}{\partial V}\right|_{x=x_0} & \left.\frac{\partial \hat{P}^G}{\partial \theta}\right|_{x=x_0} & \left.\frac{\partial \hat{P}^G}{\partial \omega}\right|_{x=x_0} \\ \left.\frac{\partial \hat{Q}^G}{\partial V}\right|_{x=x_0} & \left.\frac{\partial \hat{Q}^G}{\partial \theta}\right|_{x=x_0} & \left.\frac{\partial \hat{Q}^G}{\partial \omega}\right|_{x=x_0} \end{bmatrix}$$

$$\mathcal{J}^L(x_0) = \begin{bmatrix} \left.\frac{\partial \hat{P}^L}{\partial V}\right|_{x=x_0} & \left.\frac{\partial \hat{P}^L}{\partial \theta}\right|_{x=x_0} & \left.\frac{\partial \hat{P}^L}{\partial \omega}\right|_{x=x_0} \\ \left.\frac{\partial \hat{Q}^L}{\partial V}\right|_{x=x_0} & \left.\frac{\partial \hat{Q}^L}{\partial \theta}\right|_{x=x_0} & \left.\frac{\partial \hat{Q}^L}{\partial \omega}\right|_{x=x_0} \end{bmatrix}. \tag{9}$$

Equation (8) is useful to understand the dependencies of the model: while $\mathcal{J}^G(x)$ is determined from the designed droop control functions, $\mathcal{J}^L(x)$ is subordinated to the availability of the models of the network's loads. In the realistic case in which these models are unknown, the term is neglected and the loads are, hence, approximated as constant power. Introducing a time discretization, with time index k, so that $dx = x(k+1) - x(k)$ and $d\bar{u} = \bar{u}(k+1) - \bar{u}(k)$, the sensitivity matrix can be exploited to obtain a linearized approximation of the effect on the network variables due to small changes in the droop-controlled inverters' set points

$$\begin{aligned} x(k+1) &= x(k) + \mathcal{S}(x)\,(\bar{u}(k+1) - \bar{u}(k)) \\ &= x(k) + \mathcal{S}(x)\Delta\bar{u}(k) \end{aligned} \tag{10}$$

where, clearly, $\Delta\bar{u}$ represents the variation of vector $\bar{u}$ at time k. Recalling that $\bar{u}(k) = \bar{u}^{Gd}(k) + \bar{u}^{Gn}(k) + \bar{u}^L(k)$, (10) can be reformulated as

$$\begin{aligned} x(k+1) = x(k) &+ B(x(k))\Delta\bar{u}^{Gd}(k) \\ &+ M_{Gn}(x(k))\Delta\bar{u}^{Gn}(k) \\ &+ M_L(x(k))\Delta\bar{u}^L(k) \end{aligned} \tag{11}$$

where $B(x) \in \mathbb{R}^{2n\times 2|\mathcal{V}^{Gd}|}$, $M_{Gn}(x) \in \mathbb{R}^{2n\times 2|\mathcal{V}^{Gn}|}$, and $M_L(x) \in \mathbb{R}^{2n\times 2|\mathcal{V}^L|}$ and their columns are obtained from $\mathcal{S}(x)$ so that

$$\begin{aligned} B_{\cdot,i}(x) &= \mathcal{S}_{\cdot,j}(x)|_{j\in\mathcal{V}^{Gd}}, \quad \forall i = 1,2,\ldots,|\mathcal{V}^{Gd}| \\ M_{Gn\cdot,i}(x) &= \mathcal{S}_{\cdot,j}(x)|_{j\in\mathcal{V}^{Gn}}, \quad \forall i = 1,2,\ldots,|\mathcal{V}^{Gn}| \\ M_{L\cdot,i}(x) &= \mathcal{S}_{\cdot,j}(x)|_{j\in\mathcal{V}^{L}}, \quad \forall i = 1,2,\ldots,|\mathcal{V}^{L}| \end{aligned}$$

where $Q_{\cdot,k}$ denotes the kth column of matrix Q.

The terms $\Delta\bar{u}^{Gn}(k)$, $\Delta\bar{u}^L(k)$ referring to the variations in the nominal values of the nondispatchable production and load absorption can be used to exploit the possibility to forecast part of these data and can be considered, in such case, as known disturbances. Neglecting them, instead, corresponds to assume that no change is expected to intervene during the kth time instant.

In order to cancel the error frequency in steady-state conditions, $e_\omega(k) = \omega(k) - \omega^*$, following a standard procedure, an integral action is introduced, enlarging the state vector to include the dynamics of the new variable ε [i.e., $\varepsilon(k+1) = \varepsilon(k) + e_\omega(k+1)$].

At last, for the sake of notational simplicity, we combine the known disturbances eventually available, $\Delta\bar{u}^{Gn}$ and $\Delta\bar{u}^L$, in the vector ΔD, and drop the state dependence for the matrices obtaining

$$X(k+1) = A\,X(k) + B\,\Delta U(k) + M\,\Delta D(k) \tag{12}$$

where $\Delta U = \Delta\bar{u}^{Gd}$, and X represents the state vector enlarged with ε. The equations in (12) describe the evolution of the network variables X due to the variation of the set points ΔU of the dispatchable generators, which are the actual control variables of this system. From the values of the set points at the kth time instant, $\bar{u}^{Gd}(k)$, and assuming to know the sequence of variations for the following i time periods, $\Delta U(k), \Delta U(k+1), \ldots, \Delta U(k+i)$, the set points are easily computed as:

$$\bar{u}^{Gd}(k+i) = \bar{u}^{Gd}(k) + \sum_{j=0}^{j=i-1} \Delta U(k+j). \tag{13}$$

Since the model comprises the effect of the droop compensations, $\hat{u}^{Gd}$, the actual output of the generators is also obtained as follows:

$$u^{Gd}(k+i) = \bar{u}^{Gd}(k+i) + \mathcal{J}^{Gd}x(k+i) \tag{14}$$

where $x(k+i)$ is computed according to the dynamics in (12), and, analogously to (9), $\mathcal{J}^{Gd}(x) = d\hat{u}^{Gd}/dx$.

Optimization Problem: The secondary control action is now computed as the solution of a receding horizon MPC problem over a prediction horizon N. At each time k, the matrices $B(x(k))$, $M(x(k))$, and $\mathcal{J}^{Gd}(x(k))$ are first calculated, then, according to the cost function

$$\begin{aligned} J(k) = \sum_{i=1}^{N} &\{(V(k+i) - V^*)^T Q_V (V(k+i) - V^*) \\ &+ c_\varepsilon \varepsilon(k+i)^2\} \\ + \sum_{i=0}^{N-1} &\{(\Delta U(k+i))^T R_\Delta (\Delta U(k+i)) \\ &+ (\bar{u}^{Gd}(k+i))^T R_u (\bar{u}^{Gd}(k+i))\} \end{aligned} \tag{15}$$

the algorithm computes the solution of the following constrained optimization problem:

$$\min_{\Delta U(k:k+N-1)} J(k) \tag{16}$$

where $\Delta U(k : k+N-1)$ stands for the control sequence $\Delta U(k), \Delta U(k+1), \ldots, \Delta U(k+N-1)$, subject to the following.

1) the dynamics (12)–(14);
2) the limits of the desired ranges for voltages and frequency (i.e., $V \in [V^{\min}, V^{\max}]$ and $\omega \in [\omega^{\min}, \omega^{\max}]$);
3) the technical limitations on the requested power set points (i.e., $\bar{u}^{Gd} \in [\bar{u}^{\min}, \bar{u}^{\max}]$);
4) the operational limits of the dispatchable generation units (i.e., $u^{Gd} \in [u^{\min}, u^{\max}]$);
5) a limitation in the set point variation, expressed as

$$|\Delta U(k+i)| \leq \Delta U^{\max} \quad \forall i = 0, 1, \ldots, N-1. \quad (17)$$

The cost function (15) has a double purpose: the weights on the state variables aim to reduce the difference between these variables and their nominal values, while the weight matrices R_u and R_Δ must be chosen to define a priority for the usage of the different generators. As the examples in Section III show, the introduction of these degrees of freedom in the optimization problem enhances the flexibility, allowing the definition of different energy management strategies.

Constraint (17) is meant to restrain the excursion of the input and state variables so as to partially compensate for the error systematically introduced by the decision to drop the dependence from x for the matrices B and M in (12), and for $\mathcal{J}^{Gd}$ in (14). It should be noted, that, as illustrated in Appendix A, this decision allows formulating the MPC problem as a quadratic program subject to linear constraints. This guarantees that, as long as the weights matrix is chosen to be positive definite, the problem will converge to the solution in polynomial time. Average and worst case computational time for an example case are reported in Section III.

Once the optimal solution $\Delta U(k : k+N-1)$ has been computed, according to the so-called receding horizon principle, only its first component $\Delta U(k)$ is applied, and the overall procedure is repeated at the next time instant $k+1$.

Implementing the secondary layer by means of a model predictive algorithm has the significant advantages to: 1) enable the controller to account for peculiar specifications of the MG devices (e.g., to introduce limitation on the charge/discharge rate, as well as on the SOC range, of any electrical storage devices in order to preserve its life-expectancy); 2) to readily include, as shown in (11), forecasted profiles in the computation (whether they are load or generation profiles); and 3) to allow the introduction of multiple device management strategies. The following simulation study is finalized to show the potential of this approach.

III. Simulation Study

A. Overview of the System

We consider a model of an MG consistent with the *test facility* (TF) available at Ricerca Sistema Energetico (RSE S.p.A.) As Fig. 1 shows, the TF corresponds to a small network of 13 nodes, and it is equipped with one dispatchable generator (i.e., a natural gas cogenerator identified as G), three storage systems (i.e., batteries denoted as B1, B2, and B3), two renewable source generators (i.e., a photovoltaic system and a small wind turbine, denoted as PV and WT, respectively) and two electrical loads (L1 and L2). Three constant-power loads (AUX1, AUX2, and AUX3) are also considered to take into account the power

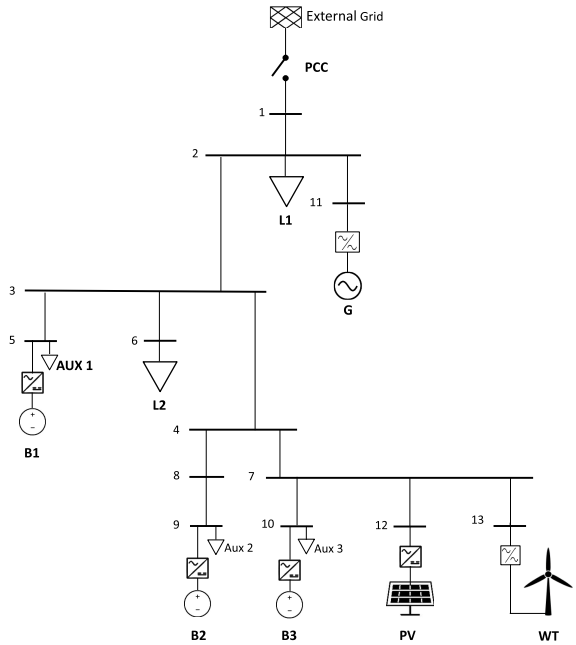

Fig. 1. TF schematic.

TABLE I
Network Admittances

$y_{1,2}$	$139.2 - j21.3$ S	$y_{4,7}$	$5.51 - j0.14$ S
$y_{2,3}$	$19.32 - j1.2$ S	$y_{4,8}$	$119.3 - j18.5$ S
$y_{2,11}$	$65.19 - j4.07$ S	$y_{7,10}$	$5376.5 - j855.7$ S
$y_{3,4}$	$52.15 - j3.26$ S	$y_{7,12}$	$5402.7 - j770$ S
$y_{3,5}$	$97.43 - j7.36$ S	$y_{7,13}$	$5376.5 - j855.7$ S
$y_{3,6}$	$63.67 - j3.20$ S	$y_{8,9}$	$54.2 - j7.7$ S

drained by the auxiliary cooling systems of the batteries. Table I collects the values of the admittance y_{ij} of the network lines $(i, j) \in \mathcal{E}$ at nominal conditions, i.e., $\omega^* = 50$ Hz. Each generation unit is interfaced to the TF by means of an inverter endowed with a primary controller which, accordingly to the *resistive* nature of the network, enforces the control law (4). Depending on the nature of the source, different *droop* configurations have been designed, so that the power variations can be consistent with the generator characteristics. The reference frequency for the network is $\omega^* = 50$ Hz, and the acceptable range is $[49.5, 50.5]$ Hz, while the security range for the nodal voltages is $[360, 440]$ V with a nominal value of $V^* = 400$ V. These values are consistent with the current Italian regulamentation for physical islands, [23]. The secondary control loop is supposed to work at a sampling time $\tau_s = 1$ min.

Before illustrating the numerical results, a brief description of the models and the parameters adopted in the following simulations is given.

a) Storage units: Due to the fast inverter interface, B1, B2, and B3 are assumed to instantaneously provide the requested power. The output active and reactive powers are limited according to a rectangular capability curve, meaning that they must respect maximum and minimum limits while no restriction is imposed to the power factor (i.e., $P_B \in [P_{\min}, P_{\max}]$ and $Q_B \in [Q_{\min}, Q_{\max}]$).

TABLE II
STORAGE UNITS PARAMETERS

	C^{tot}	$Pmax$	$Pmin$	$Qmax$	$Qmin$
B1	30 kWh	30 kW	−11 kW	60 kVar	−60 kVar
B2	32 kWh	25 kW	−25 kW	15 kVar	−15 kVar
B3	55 kWh	12 kW	−9 kW	13 kVar	−11 kVar

The dynamics of the SOCs are considered as well, due to their relevance for an efficient resource management strategy. The model adopted is the following:

$$\mathrm{SOC}(k+1) = (1-\lambda)\mathrm{SOC}(k) - \frac{\tau_s}{C_B} P_B(k)$$

where the value of SOC is normalized, λ represents a proportional loss of charge, and C_B stands for the nominal capacity of the battery. Operational bounds are also introduced in order to preserve the life-expectancy of the devices: it is required that $0.15 \leq \mathrm{SOC} \leq 0.9$, which is added to the secondary control algorithm as a soft constraint. The model parameters of the TF's storage units are listed in Table II, where the limits of the capability curves are also used to compute the droop coefficient as in (5).

b) Controllable generator: Similar to the batteries, the generator G has been supposed to instantaneously deliver the requested power output. A linear hull of its nonconvex capability region has been considered to define the operational limits of the model of this rotating generator. The corresponding constraints take the form

$$\begin{aligned} 0 \text{ kW} \leq P_G &\leq 50 \text{ kW} \\ -40 \text{ kVar} \leq Q_G &\leq 40 \text{ kVar} \\ \frac{P_G}{\tan(\arccos(0.2))} \leq Q_G &\leq \frac{P_G}{\tan(\pi - \arccos(0.2))} \end{aligned}$$

where 0.2 corresponds to the value of the minimum power factor allowed by the generator unit.

Once again, the primary control parameters are defined as in (5).

c) Renewable energy sources: Renewable energy generators are subject, in many countries, to specific regulations aiming to maximize their zero-emissions production. Consistently, in these simulations, we adopted a droop control function properly modified to take into account the impossibility to further increase the production as well as to limit the chance to modulate the active power production when the voltage reaches critical levels. To this purpose, denoting (with a small abuse of the notation) by P_{Gn} the active power produced by any of the two nondispatchable generators, by $\bar{P}_{Gn}$ the potential power production of the unit, and by V the voltage measured at the node, we adopted the droop control function

$$P_{Gn} = \begin{cases} \bar{P}_{Gn}, & \text{if } V \leq \tilde{V} \\ \bar{P}_{Gn} + m^V (V - V^*), & \text{if } \tilde{V} < V \end{cases}$$

where $\tilde{V} = 420$ V represents the threshold after which it is possible to reduce the power production, and the droop coefficient is computed as $m^V = -\bar{P}_{Gn}/(V^{\max} - \tilde{V})$. In this case, the droop coefficient m^V is not constant, since it depends on the actual power potentially delivered by the nondispatchable generator. Concerning the reactive power, the primary control has been defined as in (3), with the droop coefficient computed as in (5), considering $Q^{\max} = 10$ kVar and $Q^{\min} = -10$ kVar.

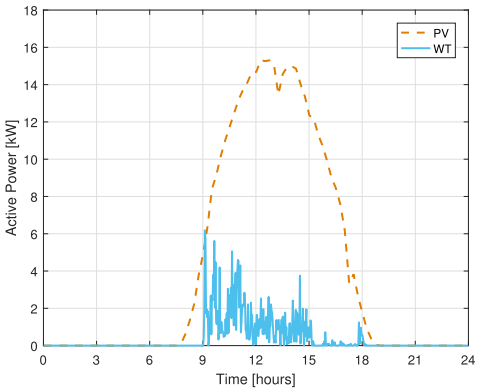

Fig. 2. Renewable sources power production profiles.

TABLE III
LOAD MODEL PARAMETERS

	k_{pv}	$k_{p\omega}$	k_{qv}	$k_{q\omega}$
L1	1.4	5.3	1.4	4.1
L2	1.2	0.7	2.7	-2.3

To simulate the values of $\bar{P}_{Gn}$ for both PV and WT, we used real data collected at the RSE TF. Fig. 2 shows their profiles.

d) Loads: To define the dynamics of the loads, we adopted two nonlinear models available in the literature: L1 corresponds to an agricultural water pump (described in [24]), while L2 represents an aggregate residential load (as in [25]). The model equations are reported in (18) and (19), respectively, while the parameters are collected in Table III

$$\begin{cases} P = P^* \left(\dfrac{V}{V^*}\right)^{k_{pv}} \left(\dfrac{\omega}{\omega^*}\right)^{k_{p\omega}} \\ Q = Q^* \left(\dfrac{V}{V^*}\right)^{k_{qv}} \left(\dfrac{\omega}{\omega^*}\right)^{k_{q\omega}} \end{cases} \tag{18}$$

$$\begin{cases} P = P^* \left(\dfrac{V}{V^*}\right)^{k_{pv}} (1 + k_{p\omega}(\omega - \omega^*)) \\ Q = Q^* \left(\dfrac{V}{V^*}\right)^{k_{qv}} (1 + k_{q\omega}(\omega - \omega^*)). \end{cases} \tag{19}$$

It is worth noticing that the agricultural water pump is a rotating load, consequently characterized by an inductive behavior (as shown by the value of its $k_{p\omega}$ parameter). This relationship is in contrast with the implemented resistive droop configuration. The nominal profiles, i.e., the active power absorbed by the loads under nominal conditions (V^*, ω^*), together with the variations in its power factor, are shown in Fig. 3. Finally, AUX1, AUX2, and AUX3 are supposed to absorb constant active and reactive power, whose values are reported in Table IV.

e) Secondary layer implementation: The centralized secondary controller has been implemented according to the approach reported in Section II-B. The optimization is performed taking into account a prediction horizon of 15 min,

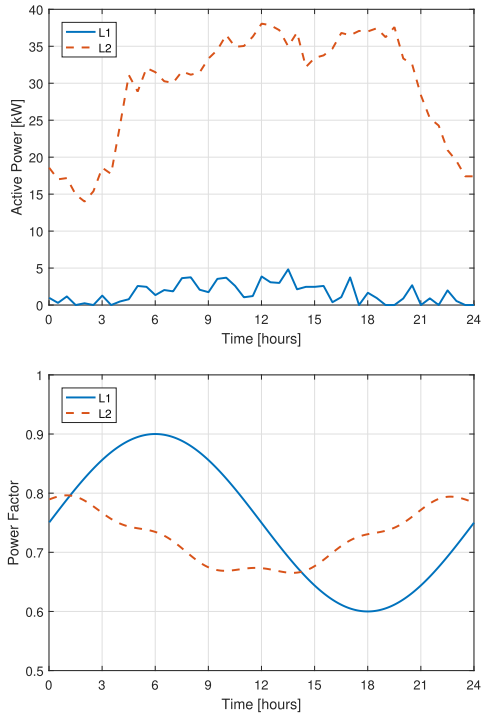

Fig. 3. Load power absorption and power factor profiles.

TABLE IV
PARAMETERS OF THE AUXILIARY LOADS

	P	Q
AUX 1	4.50 kW	−4.96 kVar
AUX 2	0.19 kW	−2.12 kVar
AUX 3	0.28 kW	−0.83 kVar

i.e., $N = 15$. The value of N has been chosen through several tests as a good compromise between the desired performances and a limited modeling error due to the assumption that the matrices B, M_{Gn}, and M_L in (11) are constant over the prediction horizon. Regarding the cost function, the weighting matrices of the cost function adopted in the simulations are collected in Appendix B.

In order to test the control system in a realistic setting, where the network parameters description is seldom accurate, we provided the model-based secondary controller with incorrect values of the lines' impedances. In particular, we modified the values of the impedance of the (i, j) line, $\bar{Z}_{ij}$, introducing a random Gaussian error $e \sim WGN(0, 0.5)$ and letting $\bar{Z}_{ij} = (1 + e)\bar{Z}_{ij}$, $\forall (i, j) \in \mathcal{E}$ be the values adopted by the MPC controller for the modeling of the system.

B. Results

Two examples are presented in this section. First, we show the differences of the behavior of the controlled system with and without the secondary layer control action. In the second scenario, two simple energy management strategies are described and tested.

f) Example 1: The TF is considered to be operated in islanded condition in time interval (17:00, 18:00). To test the effectiveness of the secondary layer, L2 is supposed to suddenly absorb additional 15 kW between 17:30 and 17:40, as shown in Fig. 4. The initial SOCs of batteries are set such that $\text{SOC}_{B1} = \text{SOC}_{B2} = 17\%$, while $\text{SOC}_{B3} = 70\%$.

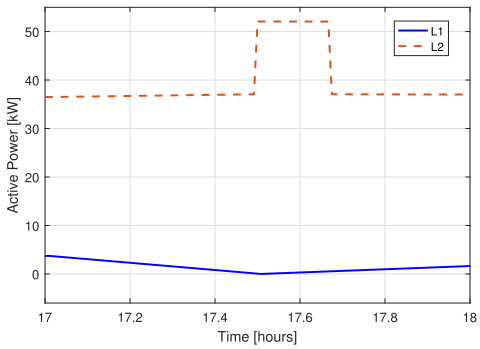

Fig. 4. Example 1: active power trends of L1 and L2 between 17:00 and 18:00.

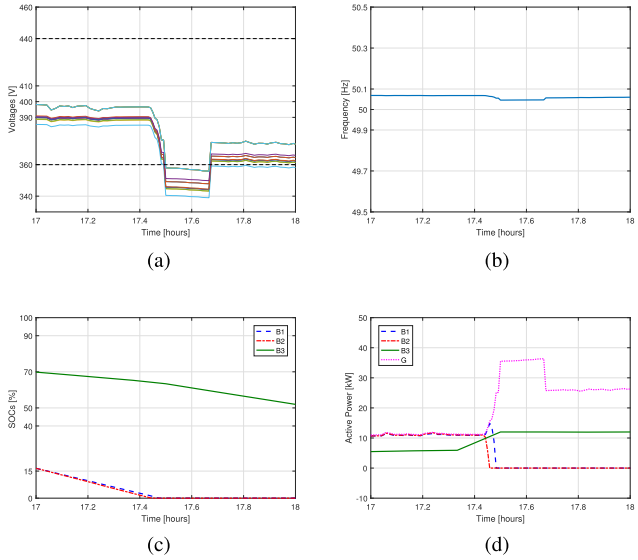

Fig. 5. Example 1: responses of the network controlled by the sole primary control layer. (a) Nodal voltages. (b) Frequency. (c) SOCs. (d) Active power.

Fig. 5 collects the response of the network simulator to the sole action of the primary control layer. The nodal voltages and the frequency transients are shown in Fig. 5(a) and (b), respectively, while Fig. 5(c) shows the levels of SOC of the batteries, and Fig. 5(d) presents the active power production profiles. It is evident that the distributed proportional controllers modulate the sources' production making the network variables to evolve close to their allowed ranges. The control system, however, fails in keeping the nodal voltages inside the regulation bounds because of the load peak and of the complete discharge of B1 and B2. As expected, also the frequency does not converge to its nominal value. Fig. 5 shows how, although a fast primary layer is necessary to promptly reduce the power unbalances, an accurate distribution and a high-level coordination of the power production would also be beneficial for the system. Furthermore, the requirement to properly manage the batteries' SOCs suggests the need of a resource management strategy.

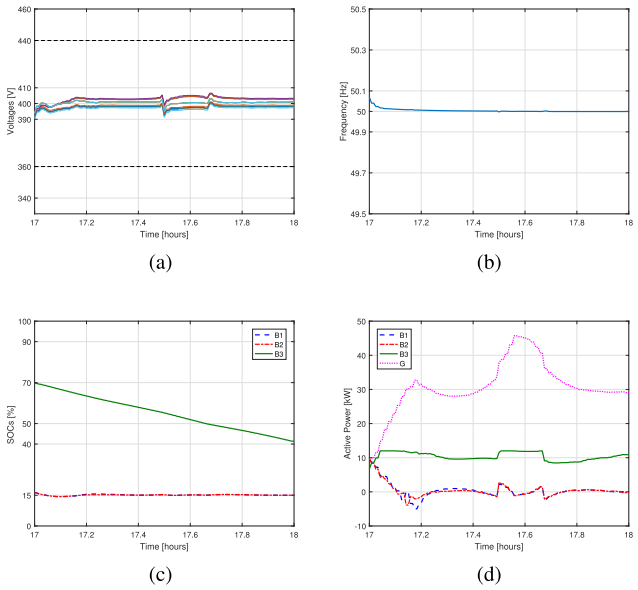

Fig. 6. Example 1: responses of the network controlled by the proposed hierarchical structure. (a) Nodal voltages. (b) Frequency. (c) SOCs. (d) Active power.

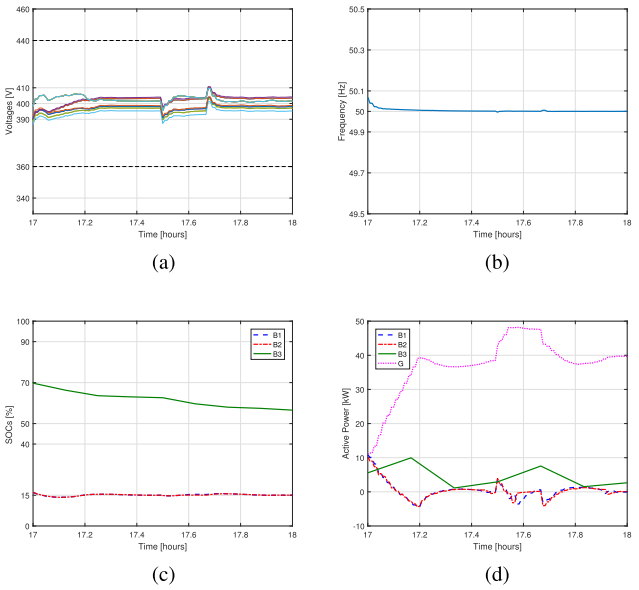

Fig. 8. Example 1: responses of the network controlled by the proposed hierarchical structure in case forecasts are not known. (a) Nodal voltages. (b) Frequency. (c) SOCs. (d) Active power.

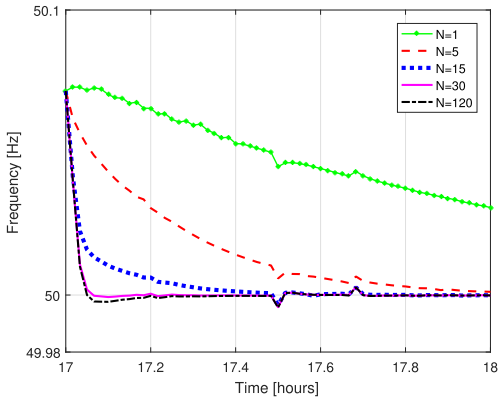

Fig. 7. Example 1: frequency transient with respect to prediction horizon variations.

As shown in Fig. 6, the introduction of the presented secondary control scheme corresponds to a significant improvement of the network behavior; in fact, after a transient, both the frequency and the nodal voltages shortly reach their nominal values, maintaining the references also when the L2 load peak occurs. Finally, thanks to the defined constraints, it is evident that the secondary layer manages to keep the SOCs inside the recommended limits as requested.

In Fig. 7, the frequency transient is shown in order to examine the sensibility of the system with respect to the variation of the prediction horizon. It is possible to notice that $N = 15$ is an acceptable compromise with respect to the desired behavior of the system. If high values of the prediction horizon are taken, it should be considered that the modeling error will increase, since predicted variables move further from the linearization point. This effect could be more significant if more complex networks are taken into account.

It is worth noticing that in Fig. 6, the power profiles of loads and renewable sources are supposed to be available to the secondary layer, meaning that the control structure knows how the uncontrollable power trends vary during the next 15 min. Since this data are usually unknown or not accurate, the hierarchical control structure is also tested without relying on these forecasts. As shown in Fig. 8, also in this case, the described control objectives are satisfied with the only small drawback that the voltages are sightly more perturbed by the sudden load peak.

g) Example 2: Although the principal objective of the secondary layer is to minimize the network variables' deviations, the flexibility of the MPC approach allows to implement different resource management policies; to show this feature, two different strategies have been tested aiming to prioritize the use of some sources with respect to others. In the following simulations, the initial SOCs are set such that $\mathrm{SOC}_{B1} = 90\%$, $\mathrm{SOC}_{B2} = 75\%$, and $\mathrm{SOC}_{B3} = 60\%$, while the power trends of nondispatchable generation and loads are considered unknown. The first strategy, denoted "economic resource management," aims to reduce the fuel consumption due to the cogenerator, prioritizing the usage of the batteries; this strategy may potentially be adopted in a scenario in which the MG is expected to operate in islanded mode for a limited amount of time and, therefore, containing the costs might be a goal. Fig. 9 shows the results of the implementation of this strategy taking into account 1 h of islanded operation, precisely between 20:00 and 21:00. As it is possible to notice from Fig. 9(d), the contribution of G is restrained for the whole simulation, while most of the power is produced by batteries, which, as shown in Fig. 9(c), show consistent discharges.

An opposite logic, defined "Reliable Resource Management," is also tested. In a scenario in which the islanded condition might be prolonged for a considerable amount of time, it would be intuitively better to prioritize the production from G, while maintaining the possibility

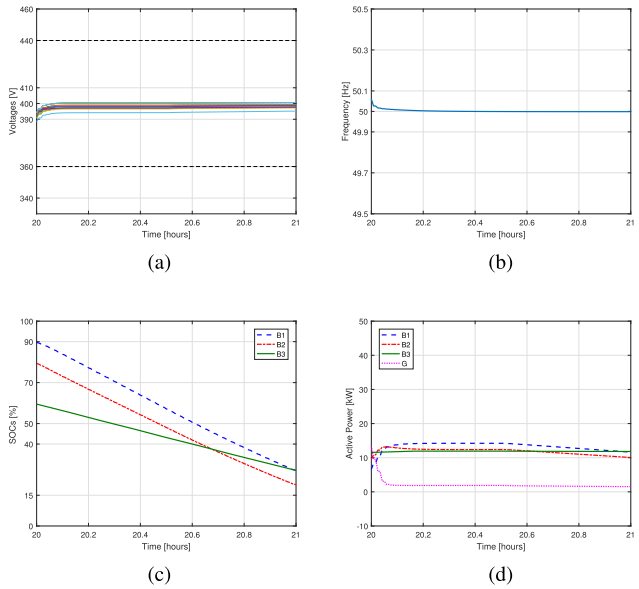

Fig. 9. Example 2: responses of the network with the economic resource management strategy. (a) Nodal voltages. (b) Frequency. (c) SOCs. (d) Active power.

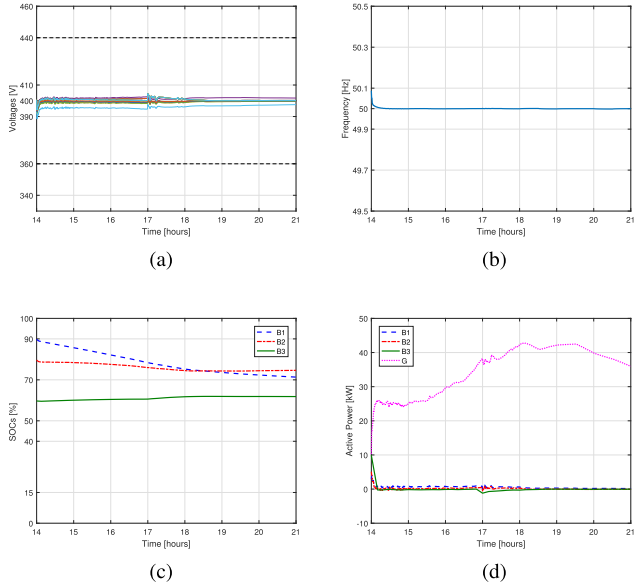

Fig. 10. Example 2: responses of the network with the reliable resource management strategy. (a) Nodal voltages. (b) Frequency. (c) SOCs. (d) Active power.

to increase the production with the batteries only when necessary. Simulating the islanded condition for 7 h, i.e., between 14:00 and 21:00, Fig. 10 shows how this approach allows to preserve the batteries' SOCs, while the generator G delivers most of the power necessary to satisfy the loads. Clearly, the "economic" and the "reliable" strategies presented in this paper represent simple policies meant to prioritize one or the other type of generation; nevertheless, they represent a valuable example to testify the flexibility of the approach and the possibility that it offers to take higher level logics into account, while keeping voltages and frequency close to their nominal values.

The secondary controller, implemented in MATLAB, on a machine equipped with an Intel dual-core processor (2.5 GHz) and 8-Gb of RAM, required on average 0.174 s to compute the solution of problem (16), and 0.322 s in the worst case. This is perfectly consistent with the defined control period.

IV. Conclusion

This paper has presented a hierarchical control structure of MGs in islanded operation. A decentralized droop control is employed as primary layer. Its objective is to cope with the network unbalances, rejecting the voltages and frequency fluctuations due to the unpredictability of load and nondispatchable generation.

A secondary control layer based on the MPC approach has also been described. After a derivation of the model, we have formulated the problem as a constrained optimization program, showing how this method allows considering both the acceptable range of the network variables and the capability of the generators, in the definition of the control action. The possibility to delineate an energy management strategy is also demonstrated.

The results of the simulation experiments show the potentialities as well as the flexibility of the approach.

Appendix A
Optimization Problem in Quadratic Form

In this section, the formulation of (16) in the standard quadratic form

$$\min_z \{z^\top \mathcal{Q} z + c^\top z\}, \quad \text{s.t. } \mathcal{A} z = b \wedge \mathcal{C} z \leq d \tag{20}$$

is presented. The relation with respect to (16) if derived step by step, starting from the constraints formulation.

The following notations are adopted.

1) I_i stands for the identity matrix with dimensions (i, i).
2) $\mathbb{1}_{i,j}$ defines the ones matrix with dimensions (i, j).
3) $\mathbf{0}_{i,j}$ represents the zeros matrix with dimensions (i, j).
4) n and m stand, respectively, for the number of nodes (consistently with the previous notation) and the number of the available dispatchable generators (*i.e.*, $m = |\mathcal{V}^{Gd}|$).
5) p denotes the number of state variables, i.e., $p = 2n+1$.
6) The symbol $\otimes$ represents the Kronecker product operator.

A. Equality Constraint

Introducing vectors

$$\begin{aligned}
\tilde{X} &= [X(k+1)^\top, X(k+2)^\top, \ldots, X(k+N)^\top]^\top \\
\tilde{\Delta U} &= [\Delta U(k)^\top, \Delta U(k+1)^\top, \ldots, \Delta U(k+N-1)^\top]^\top \\
\tilde{\Delta D} &= [\Delta D(k)^\top, \Delta D(k+1)^\top, \ldots, \Delta D(k+N-1)^\top]^\top
\end{aligned}$$

and following the standard MPC approach, it is possible to rewrite equation (12) as:

$$\tilde{X} = \tilde{A} X(k) + \tilde{B} \tilde{\Delta U} + \tilde{M} \tilde{\Delta D} \tag{21}$$

where $\tilde{A}$, $\tilde{B}$, and $\tilde{M}$ are obtained as

$$\tilde{A} = \begin{bmatrix} A \\ A^2 \\ \dots \\ A^N \end{bmatrix}$$

$$\tilde{B} = \begin{bmatrix} B & 0 & 0 & \dots & 0 & 0 \\ AB & B & 0 & \dots & 0 & 0 \\ \dots & \dots & \dots & \dots & \dots & \dots \\ A^{N-2}B & A^{N-3}B & A^{N-4}B & \dots & B & 0 \\ A^{N-1}B & A^{N-2}B & A^{N-3}B & \dots & AB & B \end{bmatrix}$$

$$\tilde{M} = \begin{bmatrix} M & 0 & 0 & \dots & 0 & 0 \\ AM & M & 0 & \dots & 0 & 0 \\ \dots & \dots & \dots & \dots & \dots & \dots \\ A^{N-2}M & A^{N-3}M & A^{N-4}M & \dots & M & 0 \\ A^{N-1}M & A^{N-2}M & A^{N-3}M & \dots & AM & M \end{bmatrix}.$$

Furthermore, defining

$$\bar{U} = [\bar{u}^{Gd}(k+1)^\top, \bar{u}^{Gd}(k+2)^\top, \dots, \bar{u}^{Gd}(k+N)^\top]^\top$$
$$U = [u^{Gd}(k+1)^\top, u^{Gd}(k+2)^\top, \dots, u^{Gd}(k+N)^\top]^\top$$

alternative formulations of (13) and (14) are, respectively, given by

$$\bar{U} = \mathbb{1}_{N,1} \otimes \bar{u}^{Gd}(k) + \mathcal{L}\Delta\tilde{U} \tag{22}$$
$$U = \bar{U} + (I_N \otimes \mathcal{J}^{Gd})\tilde{X} \tag{23}$$

where $\mathcal{L}$ is a lower triangular matrix of ones with dimensions $(2mN, 2mN)$.

Letting $z = [\tilde{X}^\top \Delta\tilde{U}^\top \bar{U}^\top U^\top]^\top$ represent the vector containing the optimization variables of (20), (21)–(23) may be, hence, grouped to express the equality constraint with $\mathcal{A}$ and b computed as

$$\mathcal{A} = \begin{bmatrix} I_{pN} & -\tilde{B} & \mathbf{0}_{pN,2mN} & \mathbf{0}_{pN,2mN} \\ \mathbf{0}_{pN,pN} & -\mathcal{L} & I_{2mN} & \mathbf{0}_{2mN,2mN} \\ -I_N \otimes \mathcal{J}^{Gd} & \mathbf{0}_{2mN,2mN} & -I_{2mN} & I_{2mN} \end{bmatrix}$$

$$b = \begin{bmatrix} \tilde{A}X(k) + \tilde{M}\Delta\tilde{D} \\ \mathbb{1}_{N,1} \otimes \bar{u}^{Gd}(k) \\ \mathbf{0}_{2mN,1} \end{bmatrix}.$$

B. Inequality Constraint

Recalling that $X = [V^\top \theta^\top \omega\varepsilon]^\top$, to define the inequality constraint, the following matrices are first introduced:

$$c_V = [I_n \quad \mathbf{0}_{n,n+1}]$$
$$c_\omega = [\mathbf{0}_{1,2n-1} \quad 1 \quad 0].$$

The constraints concerning the variables' bounds in (16) may then be expressed as the single inequality constraint in (20) considering

$$\mathcal{C} = \begin{bmatrix} I_N \otimes c_V & \mathbf{0}_{nN,2mN} & \mathbf{0}_{nN,2mN} & \mathbf{0}_{nN,2mN} \\ -I_N \otimes c_V & \mathbf{0}_{nN,2mN} & \mathbf{0}_{nN,2mN} & \mathbf{0}_{nN,2mN} \\ I_N \otimes c_\omega & \mathbf{0}_{N,2mN} & \mathbf{0}_{N,2mN} & \mathbf{0}_{N,2mN} \\ -I_N \otimes c_\omega & \mathbf{0}_{N,2mN} & \mathbf{0}_{N,2mN} & \mathbf{0}_{N,2mN} \\ \mathbf{0}_{2mN,pN} & \mathbf{0}_{2mN,2mN} & I_{2mN,2mN} & \mathbf{0}_{2mN,2mN} \\ \mathbf{0}_{2mN,pN} & \mathbf{0}_{2mN,2mN} & -I_{2mN,2mN} & \mathbf{0}_{2mN,2mN} \\ \mathbf{0}_{2mN,pN} & \mathbf{0}_{2mN,2mN} & \mathbf{0}_{2mN,2mN} & I_{2mN,2mN} \\ \mathbf{0}_{2mN,pN} & \mathbf{0}_{2mN,2mN} & \mathbf{0}_{2mN,2mN} & -I_{2mN,2mN} \\ \mathbf{0}_{2mN,pN} & I_{2mN,2mN} & \mathbf{0}_{2mN,2mN} & \mathbf{0}_{2mN,2mN} \\ \mathbf{0}_{2mN,pN} & -I_{2mN,2mN} & \mathbf{0}_{2mN,2mN} & \mathbf{0}_{2mN,2mN} \end{bmatrix}$$

TABLE V
WEIGHTS ADOPTED IN THE SIMULATION EXAMPLES

	Example 1	Example 2 Economic Management	Example 2 Reliable Management
c_ε	10^8	10^8	10^8
w_v	10^5	10^5	10^5
$w_{\Delta P1}$	1	1	1
$w_{\Delta Q1}$	1	1	1
$w_{\Delta P2}$	1	1	1
$w_{\Delta Q2}$	1	1	1
$w_{\Delta P3}$	1	1	1
$w_{\Delta Q3}$	1	1	1
$w_{\Delta P4}$	1	1	1
$w_{\Delta Q4}$	1	1	1
w_{P1}	10^{-1}	10^{-1}	10^5
w_{Q1}	1	1	1
w_{P2}	10^{-1}	10^{-1}	10^5
w_{Q2}	1	1	1
w_{P3}	10^{-3}	10^{-5}	10^5
w_{Q3}	1	1	1
w_{P4}	10^{-3}	10	10^{-3}
w_{Q4}	1	1	1

and

$$d = \begin{bmatrix} \mathbb{1}_{N,1} \otimes V^{\max} \\ -\mathbb{1}_{N,1} \otimes V^{\min} \\ \mathbb{1}_{N,1} \cdot \omega^{\max} \\ -\mathbb{1}_{N,1} \cdot \omega^{\min} \\ \mathbb{1}_{N,1} \cdot \bar{u}^{\max} \\ -\mathbb{1}_{N,1} \cdot \bar{u}^{\min} \\ \mathbb{1}_{N,1} \cdot u^{\max} \\ -\mathbb{1}_{N,1} \cdot u^{\min} \\ \mathbb{1}_{N,1} \cdot \Delta U^{\max} \\ -\mathbb{1}_{N,1} \cdot \Delta U^{\min} \end{bmatrix}.$$

C. Cost Function

Considering Q_V, R_Δ, and R_u to be diagonal (consisting with the standard practice), and defining $\overline{w}_V$, $\overline{w}_\Delta$, and $\overline{w}_u$ as the vectors containing the corresponding diagonal values (i.e., $Q_V = \text{diag}\{\overline{w}_V\}$, $R_\Delta = \text{diag}\{\overline{w}_\Delta\}$, and $R_u = \text{diag}\{\overline{w}_u\}$), the cost function of (20) is finally defined by

$$\mathcal{Q} = \text{diag}\{\mathbb{1}_{1,N} \otimes q_x \quad \mathbb{1}_{1,N} \otimes \overline{w}_\Delta \quad \mathbb{1}_{1,N} \otimes \overline{w}_u \quad \mathbf{0}_{1,2mN}\}$$
$$c^\top = [\mathbb{1}_{1,N} \otimes q_\omega \quad \mathbf{0}_{1,6mN}]$$

where

$$q_x = [\overline{w}_V \quad \mathbf{0}_{1,n} \quad c_\varepsilon]$$
$$q_\omega = [-2\overline{w}_V \cdot V^* \quad \mathbf{0}_{1,n+1}].$$

APPENDIX B
WEIGTHING MATRICES

The weighting matrices implemented in (15) are diagonal, and they are composed as the following:

$$Q_V = \text{diag}\{w_v, \dots, w_v\}$$
$$R_\Delta = \text{diag}\{w_{\Delta P1}, w_{\Delta Q1}, \dots, w_{\Delta Png}, w_{\Delta Qng}\}$$
$$R_u = \text{diag}\{w_{P1}, w_{Q1}, \dots, w_{Png}, w_{Qng}\}$$

where ng corresponds to the number of controllable generators ordered according to the following sequence:

$\{B1, B2, B3, G\}$. The matrices' parameters implemented in (15) for the different simulation examples are reported in Table V.

ACKNOWLEDGMENT

The authors would like to thank E. Corsetti, A. Guagliardi, M. Rossi, and A. Villa (RSE S.p.A.) for fruitful discussions and suggestions.

REFERENCES

[1] D. E. Olivares *et al.*, "Trends in microgrid control," *IEEE Trans. Smart Grid*, vol. 5, no. 4, pp. 1905–1919, Jul. 2014.
[2] M. C. Chandorkar, D. M. Divan, and R. Adapa, "Control of parallel connected inverters in standalone AC supply systems," *IEEE Trans. Ind. Appl.*, vol. 29, no. 1, pp. 136–143, Jan./Feb. 1993.
[3] J. W. Simpson-Porco, F. Dorfler, F. Bullo, Q. Shafiee, and J. M. Guerrero, "Stability, power sharing, & distributed secondary control in droop-controlled microgrids," in *Proc. IEEE Int. Conf. Smart Grid Commun. (SmartGridComm)*, Oct. 2013, pp. 672–677.
[4] J. Schiffer, R. Ortega, A. Astolfi, J. Raisch, and T. Sezi, "Stability of synchronized motions of inverter–based microgrids under droop control," in *Proc. 19th IFAC World Congr.*, 2014, pp. 6361–6367.
[5] K. De Brabandere, B. Bolsens, J. Van den Keybus, A. Woyte, J. Driesen, and R. Belmans, "A voltage and frequency droop control method for parallel inverters," *IEEE Trans. Power Electron.*, vol. 22, no. 4, pp. 1107–1115, Jul. 2007.
[6] Y. W. Li and C.-N. Kao, "An accurate power control strategy for power-electronics-interfaced distributed generation units operating in a low-voltage multibus microgrid," *IEEE Trans. Power Electron.*, vol. 24, no. 12, pp. 2977–2988, Dec. 2009.
[7] D. Wu, J. M. Guerrero, J. C. Vasquez, T. Dragicevic, and F. Tang, "Coordinated power control strategy based on primary-frequency-signaling for islanded microgrids," in *Proc. IEEE Energy Convers. Congr. Expo. (ECCE)*, Sep. 2013, pp. 1033–1038.
[8] T. Vandoorn, J. D. M. De Kooning, B. Meersman, and L. Vandevelde, "Review of primary control strategies for islanded microgrids with power-electronic interfaces," *Renew. Sustain. Energy Rev.*, vol. 19, pp. 613–628, Mar. 2013.
[9] J. W. Simpson-Porco, Q. Shafiee, F. Dörfler, J. C. Vasquez, J. M. Guerrero, and F. Bullo, "Secondary frequency and voltage control of islanded microgrids via distributed averaging," *IEEE Trans. Ind. Electron.*, vol. 62, no. 11, pp. 7025–7038, Nov. 2015.
[10] A. Bidram, F. L. Lewis, and A. Davoudi, "Distributed control systems for small-scale power networks: Using multiagent cooperative control theory," *IEEE Control Syst. Mag.*, vol. 34, no. 6, pp. 56–77, Dec. 2014.
[11] D. Wu, T. Dragicevic, J. C. Vasquez, J. M. Guerrero, and Y. Guan, "Secondary coordinated control of islanded microgrids based on consensus algorithms," in *Proc. IEEE Energy Convers. Congr. Expo. (ECCE)*, Sep. 2014, pp. 4290–4297.
[12] A. Madureira, C. Moreira, and J. P. Lopes, "Secondary load-frequency control for microgrids in islanded operation," *Renew. Energy Power Quality J.*, vol. 1, no. 3, pp. 482–486, Mar. 2005.
[13] J. A. P. Lopes, C. L. Moreira, and A. G. Madureira, "Defining control strategies for microgrids islanded operation," *IEEE Trans. Power Syst.*, vol. 21, no. 2, pp. 916–924, May 2006.
[14] J. M. Guerrero, J. C. Vasquez, J. Matas, L. G. de Vicuna, and M. Castilla, "Hierarchical control of droop-controlled AC and DC microgrids—A general approach toward standardization," *IEEE Trans. Ind. Electron.*, vol. 58, no. 1, pp. 158–172, Jan. 2011.
[15] J. J. Grainger and W. D. Stevenson, *Power System Analysis*. New York, NY, USA: McGraw-Hill, 1994.
[16] D. Wu, F. Tang, J. C. Vasquez, and J. M. Guerrero, "Control and analysis of droop and reverse droop controllers for distributed generations," in *Proc. 11th Int. Multi-Conf. Syst. Signals Devices (SSD)*, Feb. 2014, pp. 1–5.
[17] A. Villa, F. Belloni, and C. Gandolfi, "Caratterizzazione sperimentale del comportamento di una porzione della test facility durante il funzionamento in isola elettrica e studio delle interazioni tra generatori statici con controllo droop in isola," RSE S.P.A., Milan, Italy, Tech. Rep. 14000427, Feb. 2014.
[18] J. W. Simpson-Porco, F. Dörfler, and F. Bullo, "Synchronization and power sharing for droop-controlled inverters in islanded microgrids," *Automatica*, vol. 49, no. 9, pp. 2603–2611, 2013.
[19] A. Villa, "Sviluppo e sperimentazione del controllo locale di risorse energetiche per il funzionamento in isola della test facility di RSE," RSE S.P.A., Milan, Italy, Tech. Rep. 13000512, Jan. 2013.
[20] G. Valverde and T. Van Cutsem, "Model predictive control of voltages in active distribution networks," *IEEE Trans. Smart Grid*, vol. 4, no. 4, pp. 2152–2161, Dec. 2013.
[21] Q. Zhou and J. W. Bialek, "Generation curtailment to manage voltage constraints in distribution networks," *IET Generat. Transmiss. Distrib.*, vol. 1, no. 3, pp. 492–498, May 2007.
[22] A. Borghetti *et al.*, "Short-term scheduling and control of active distribution systems with high penetration of renewable resources," *IEEE Syst. J.*, vol. 4, no. 3, pp. 313–322, Sep. 2010.
[23] *50160-Caratteristiche Della Tensione Fornita Dalle Reti Pubbliche di Distribuzione Dellenergia Elettrica*, Comitato Elettrotecnico Italiano, Milano, Italy, 1995.
[24] R. Marconato, *Electric Power Systems*. Milano, Italy: Comitato Elettrotecnico Italiano, 2002.
[25] W. Price *et al.*, "Load representation for dynamic performance analysis," *IEEE Trans. Power Syst.*, vol. 8, no. 2, pp. 472–482, Feb. 1993.

Alessio La Bella received the B.Sc. and M.Sc. degrees in automation and control engineering from the Politecnico di Milano, Milano, Italy, in 2013 and 2015, respectively. In 2015, he also obtained the Alta Scuola Politecnica Diploma, together with the M.Sc. degree in mechatronics from the Politecnico di Torino, Torino, Italy. He is currently pursuing the Ph.D. degree in information technology with the Politecnico di Milano.

In 2016, he was with the RSE Research Center, Milan, Italy, where he was involved in the simulation of islanded electrical networks. His current research interests include optimization-based control algorithms, such as model predictive control, with a particular focus on energy and electrical applications.

Stefano Raimondi Cominesi received the B.Sc. and M.Sc. degrees in automation and control engineering from the Politecnico di Milano, Milano, Italy, in 2009 and 2012, respectively, where he is currently pursuing the Ph.D. degree with the Dipartimento di Elettronica, Informazione e Bioingegneria.

His current research interests include model-based optimization algorithms with focus on energy management problems and applications.

Carlo Sandroni received the Laurea Specialistica degree in automation engineering from the Politecnico di Milano, Milano, Italy, in 2008.

He was involved in voltage control in the distribution grid, optimization of distributed energy resources, and integration of thermal subsystems, model predictive control, and multiagent systems. He participated in different European projects, such as DERri, ERIGrid, and ELECTRA. He is currently a Researcher with the Power Generation Technologies and Materials Department, RSE S.p.A, Milan, Italy. His current research interests include smart grid control and distributed power generation.

Riccardo Scattolini was born in Milan, Italy, in 1956. He received the Laurea degree in electronic engineering from the Politecnico di Milano, Milano, Italy, in 1979.

From 1984 to 1985, he was a Visiting Researcher at the Department of Engineering Science, Oxford University, Oxford, U.K. He also spent one year in industry on the simulation and control of chemical plants. He is currently a Professor of Automatic Control with the Politecnico di Milano. His current research interests include modeling, identification, and simulation and control of industrial plants and distribution networks, with emphasis on distributed model predictive control of large-scale systems.

Mr. Scattolini received the Heaviside Premium from the Institution of Electrical Engineers, U.K., in 1991. He is currently an Associate Editor of *Automatica*.